Axial Mixing of Binary Gas Mixtures Flowing in a Random Bed of Spheres

K. W. McHENRY, JR., and R. H. WILHELM

Princeton University, *Princeton*, New Jersey

Measurements are reported on axial mixing of binary gas mixtures at room temperature and atmospheric pressure in a random bed of spherical particles. By means of the Fick's Law equation for diffusion an axial Peclet number, $d_p U/E_z$ (where d_p is particle diameter, U is interstitial velocity, and E_z is axial eddy diffusivity), was computed in terms of the ratio of the amplitudes of a sinusoidal concentration wave at the inlet and outlet of the bed. An experimental method was devised to eliminate end effects in the system. For the gas systems H_2—N_2 and C_2H_4—N_2 and for Reynolds numbers between 100 and 400 the mean of twenty-one determinations of axial Peclet number was 1.88 ± 0.15. This value is in excellent agreement with a value of 2.0 predicted theoretically on the assumption that the bed acts as a series of n perfect mixers, where n is the number of particles traversed between inlet and outlet.

Axial diffusivity for turbulent flow of gases among particles is about sixfold larger than radial diffusivity, previously determined. It is suggested that axial diffusivity may not, perhaps, be neglected in contacting devices, such as adsorbers and catalytic reactors.

The development of rational design methods for fixed-bed reactors, heat exchangers, and adsorbers presupposes a knowledge of the extent of fluid-phase mixing which occurs in the spaces between the packing. In pursuit of this requirement, measurements of eddy-diffusion coefficients for mixing perpendicular to the direction of flow now account for a substantial part of the literature. Made by a technique involving the determination of concentration profiles downstream from a point source of tracer material, these measurements have included liquid and gaseous systems over wide flow conditions. On the other hand, mixing in the direction of flow has received much less attention. In most design methods it is neglected because of the absence of steep axial gradients or perforce because of a lack of knowledge of the magnitude of the axial eddy diffusion coefficient involved. Recent studies by Ogburn (*10*) have indicated that such neglect may not always be justified. In studying the hydrogenation of ethylene in a fixed bed of catalyst with isothermal wall, this author found that experimentally determined axial temperature profiles showed several departures from those calculated with all major effects except axial diffusion taken into account. The initial temperature gradient was not so steep as the predicted gradient; the measured peak temperature did not reach the calculated peak; the temperature downstream of the peak fell more rapidly than was anticipated from the calculations. All three effects point to the presence of an important heat leak away from the temperature peak and hence possibly to axial mixing.

Previous literature on axial mixing includes the following studies. Danckwerts (*2*) measured an axial diffusion coefficient for the flow of water through Raschig rings at one value of Reynolds number. The method involved the response function of the system to a step change in concentration at the inlet. Using the response to a sinusoidally varying input Kramers and Alberda (*7*) determined axial mixing properties of water in a bed similar to that used by Danckwerts. Two values of flow rate were investigated in this study. Deisler and Wilhelm (*4*) reported a single value of the axial eddy diffusivity characteristic of a range of Reynolds numbers. The system was gaseous, with flow occurring through a bed of fused-alumina spheres. The frequency-response technique was employed.

Work on axial diffusion here reported was undertaken to include flow rates of laboratory and plant-scale interest. Independence of the results of the particular gases used in the experiments was established. A generalized correlation for use in fixed-bed equipment design is presented. Essentially an extension of the work of Deisler and Wilhelm (*4*), present high gas-flow-rate requirements led to experimental problems of producing, analyzing, and recording relatively high-frequency concentration waves of sinusoidal form. The earliest work of frequency response applied to mass diffusion problems is that of Winsche and Rosen (*12*).

THEORY

The first part of this discussion relates to the theory underlying the experimental method, the second, to a possible mechanistic approach to axial mixing in packed beds.

Experimental Method

When a fluid passes through the interstices of a packed bed, macroscopic particles of fluid will be subjected to splitting, acceleration, deceleration, and trapping. If these individual modes of mixing are repeated a large number of times in random order, the resulting over-all mixing process may be described by a law similar to Fick's Law for molecular diffusion. Practically, in a bed of sufficient length-to-diameter ratio and tube-to-particle ratio this law has been found to hold.

Making the assumptions listed below and combining Fick's Law with a material balance on a flowing system, one may write

$$E_z \frac{\partial^2 x}{\partial \mathrm{z}^2} - U \frac{\partial x}{\partial \mathrm{z}} = \frac{\partial x}{\partial t} \qquad (1)$$

where x is the mole fraction of one gas in a binary mixture, E_z is the eddy-diffusion coefficient for diffusion in the axial direction, U is the intergranular velocity, z is the axial coordinate, and t is time. The assumptions are (1) that x is a function of z and t only, there being no radial gradients, (2) that U is everywhere constant, and (3) that x may be related to the volumetric concentration usually used with Fick's Law through the constant molar density. The first term in Equation (1) represents migration of material along the tube axis in a diffusionlike manner, the second term represents transport due to gross flow, and the third term represents holdup.

Two boundary conditions are applied as follows: (1) at the inlet of the bed (z = 0) concentration is given by

$$x(0) = x_M + A(0) \cos \omega t \qquad (2)$$

where $x(0)$ is the inlet mole fraction, x_M is the mean mole fraction about which the concentration oscillates, $A(0)$ is the amplitude of the inlet concentration wave, and ω is the angular frequency of the oscillations; (2) at sufficiently long distance down the bed the amplitude approaches zero ($A \to 0$ as $\mathrm{z} \to \infty$). An alternate choice of boundary conditions has been reported (*7*) leading to the same approximate solution as Equation (5) below. However, those conditions chosen here seem more suitable in view of bed continuity maintained across the boundaries used in these experiments.

Introducing complex notation, one

K. W. McHenry, Jr., is at present with Standard Oil Company (Indiana), Whiting, Indiana.

assumes a solution to Equation (1) of the form

$$\mathbf{x} = \mathbf{A}e^{i\omega t} \tag{3}$$

where $\mathbf{x}$ is a complex mole fraction, the real part of which gives $x - x_M$, and $\mathbf{A}$ is a complex amplitude containing in its real part both the amplitude and the phase shift compared with $\mathbf{z} = 0$ of the concentration wave. Substitution of Equation (3) into Equation (1) yields an ordinary differential equation in $\mathbf{A}$ and $\mathbf{z}$ which may be solved by standard methods. With the introduction of boundary conditions this solution is

$$\mathbf{A} = A(0) \cdot \exp\left[1 - \left(1 + \frac{4i\omega E_z}{U^2}\right)^{1/2}\right] \frac{U\mathbf{z}}{2E_z} \tag{4}$$

Expansion of the square root leads to the following approximate solution:

$$\mathbf{A} \approx A(0) \exp\left[-\frac{i\omega \mathbf{z}}{U} - \frac{\omega^2 E_z \mathbf{z}}{U^3}\right] \tag{5}$$

Equation (5) is valid if the group $5\omega^2 E_z^2/U^4 \ll 1$. The maximum error in amplitude due to the use of Equation (5) in the present experimental work is 1.4%, well within the error of measurement.

Several pertinent dimensionless groups are defined as follows: dimensionless bed length $\mathbf{L}/d_p = L$, where $\mathbf{L}$ is the bed length and d_p the particle diameter; dimensionless frequency number $d_p\omega/U = N_f$; and Peclet number, $d_pU/E_z = N_{Pe}'$. Using these groups, substituting Equation (5) into Equation (3), and taking the real part yields

$$x(L) \approx x_M + A(0) \exp\left[-\frac{N_f^2 L}{N_{Pe}'}\right] \cdot \cos(\omega t - N_f L) \tag{6}$$

$x(L)$ is the mole fraction at bed length L, $N_f L = \phi_{calc}$ is the phase shift referred to the bed entrance, and $A(0) \exp[-N_f^2 L/N_{Pe}'] = A(L)$ is the amplitude at bed length L. The ratio of outlet to inlet amplitudes leads to the equation

$$\frac{A(L)}{A(0)} \approx \exp\left[-\frac{N_f^2 L}{N_{Pe}'}\right] \tag{7}$$

or

$$-\ln\left[\frac{A(L)}{A(0)}\right] \approx \frac{1}{N_{Pe}'} N_f^2 L \tag{8}$$

If the system is described by Equation (1) and the condition necessary to give Equation (5) is met, then a plot of $-\ln[A(L)/A(0)]$ vs. $N_f^2 L$ is a straight line through the origin, the slope being the reciprocal of the Peclet number.

Two methods for obtaining amplitude ratios for the reduction of data through Equation (8) were considered. The first is the direct method. In part I of Figure 1, devices for measuring the concentration of the flowing stream are placed at d and d' and the bed length between them, 0-L, is the length used in Equation (8). The peak-to-peak concentration difference shown by device d is taken as the amplitude $A(0)$, at point 0, and similarly with respect to device d' and point L. In practice several difficulties were encountered in using the direct method. For the determination of the concentration at point 0 (or L), the measuring device must approach infinitesimal length in the direction of flow. If it does not, the concentration determined is an average over the length of the measuring unit. No technique for measuring gas-phase concentrations in a negligible length, say less than one packing-element diameter, was available which did not require removal of the packing in the interior of the measurement section. The resulting unpacked space undoubtedly influenced flow conditions immediately downstream of d and immediately upstream of d', resulting in a false picture of the extent of axial mixing in an undisturbed section of packed bed. Finally, the boundary conditions associated with Equation (1) require a constant value of the diffusivity across the system boundaries. It is doubtful, however, that the mixing which occurs in the empty measuring sections can be described by Fick's Law, and, if it were the case, the diffusivity would not have the same value as in the adjacent packed sections.

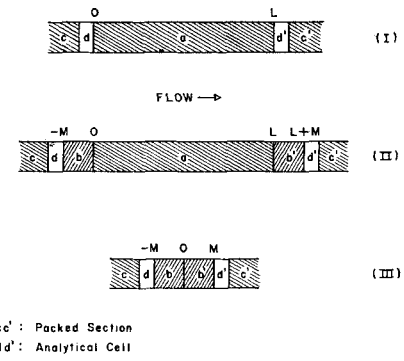

Fig. 1. Experimental arrangement of end sections and test section.

To circumvent these problems the indirect method was developed. In this method concentration-wave-amplitude measurements are made at points removed from the system boundaries and experimentally determined corrections applied to the ratios in order to identify the true amplitudes at these boundaries. Figure 1, part II, shows schematically the arrangement for measurement at points remote from the test section a, and Figure 1, part III, the arrangement for determination of corrections. The theory of the indirect method is as follows. $A(z)$ is the concentration-wave amplitude as a function of dimensionless bed length z, M is the dimensionless length of sections b and b', and ψ, a variable characterizing mixing in the analytical cells. The subscripts *in* and *out* refer to inlet and outlet and subscripts a, b, b' refer to sections in position during measurements. Then

$$A(0)_{abb'} = f[A(-M)_{abb'}, \omega, M, U, \psi_{in}] \tag{9}$$

where f is an undefined function. If the system under consideration is linear (amplitude independent), then

$$A(0)_{abb'} = A(-M)_{abb'} f_{in}(\omega, M, U, \psi_{in}) \tag{10}$$

Similarly,

$$A(L + M)_{abb'} = A(L)_{abb'} f_{out}(\omega, M, U, \psi_{out}) \tag{11}$$

or

$$A(L)_{abb'} = \frac{A(L + M)_{abb'}}{f_{out}} \tag{12}$$

Therefore

$$\left[\frac{A(L)}{A(0)}\right]_{abb'} = \left[\frac{A(L + M)}{A(-M)}\right]_{abb'} \frac{1}{f_{in} f_{out}} \tag{13}$$

when the ratio of Equations (12) and (10) is taken. The amplitude ratio at the boundaries of the test section in Equation (13) is expressed in terms of the ratio of amplitudes at points upstream and downstream of the test section and a correction factor, $1/f_{in}f_{out}$.

If the test section a is removed, then the following equations hold for the arrangement shown in Figure 1, part III:

$$A(0)_{bb'} = A(-M)_{bb'} f_{in} \tag{14}$$

and

$$A(M)_{bb'} = A(0)_{bb'} f_{out} \tag{15}$$

or

$$A(0)_{bb'} = \frac{A(M)_{bb'}}{f_{out}} \tag{16}$$

Therefore, equating the right-hand sides of Equations (14) and (16) and rearranging yields

$$\frac{1}{f_{in} f_{out}} = \left[\frac{A(-M)}{A(M)}\right]_{bb'} \tag{17}$$

Then substituting Equation (17) into Equation (13) gives

$$\left[\frac{A(L)}{A(0)}\right]_{abb'} = \left[\frac{A(L + M)}{A(-M)}\right]_{abb'} \cdot \left[\frac{A(-M)}{A(M)}\right]_{bb'} \tag{18}$$

provided that frequency ω, velocity U, length of end sections M, and the analytical-cell mixing characteristics ψ_{in} and ψ_{out} are retained at constant values during the experiments with and without the test section in place. The first three

variables are under direct control of the experimenter. The mixing characteristics of the analytical cells depend on the geometry of the cells and flow conditions within them and presumably may be kept constant from experiment to experiment. Thus the natural logarithm of Equation (18) can be substituted into Equation (8) to obtain a value of the Peclet number which characterizes axial mixing in the test section free from end effects or anomalies due to unknown amounts of mixing in the regions of the concentration-measuring devices. This method of experimentation and calculation was used in the work reported here.

Axial Mixing in Packed Beds

Any type of mixing process which is found experimentally to obey Fick's Law may be thought of as taking place as a series of individual steps repeated a large number of times. In molecular diffusion the individual step is the movement of a molecule along its mean free path, and in radial mixing in a packed bed it is the side-stepping motion of a parcel of fluid of uniform concentration as it encounters a packing element (*8*). It is useful to think of the individual step in the axial-eddy-diffusion process as a complete mixing, such as would be approached in a well-stirred vessel.

The similarity between the frequency response of a series of perfect mixers and of a system which combines plug flow and axial diffusion has already been considered by Kramers and Alberda (*7*). It is interesting to investigate this similarity more closely. The packed column may be considered to be divided into incremental lengths λ such that within each λ complete mixing occurs. The equation describing such mixing is

$$c_i = c_o + \frac{\lambda}{U}\frac{dc_o}{dt} \qquad (19)$$

where c_i is the concentration at the beginning of length λ, c_o is the uniform concentration throughout λ, and λ/U is the average residence time for length λ.

For n such mixers in series it may be shown (*9*) that for a sinusoidal input of amplitude A_0 to the first mixer, the amplitude ratio is given by

$$\ln \frac{A_n}{A_0} \approx -\frac{n\omega^2\lambda^2}{2U^2}, \qquad \frac{\omega\lambda}{U} \ll 1 \qquad (20)$$

But

$$\lambda = \frac{\mathbf{L}}{n} \qquad (21)$$

Therefore

$$\ln \frac{A_n}{A_0} \approx -\frac{\omega^2\mathbf{L}^2}{2U^2 n}, \qquad \frac{\omega\mathbf{L}}{nU} \ll 1 \qquad (22)$$

where A_n is the amplitude of the sinusoidal concentration wave leaving the nth mixer. Or, if $L = \mathbf{L}/d_p$ is substituted,

$$\ln \frac{A_n}{A_0} \approx -\frac{N_f^2 L^2}{2n}, \qquad \frac{N_f L}{n} \ll 1 \qquad (23)$$

If it is assumed that perfect mixing occurs over the length represented by one particle diameter, then

$$n = L \qquad (24)$$

and

$$-\ln \frac{A_n}{A_0} \approx \frac{N_f^2 L}{2}, \qquad N_f \ll 1 \qquad (25)$$

But the left-hand side of Equation (25) for the mixing model is identical with the left-hand side of Equation (8) for the differential equation solution. Therefore

$$N_{Pe}' = 2 \qquad (26)$$

when complete mixing is achieved at every particle position down the tube. It will be shown that this value of N_{Pe}' is secured quite closely through experiment.

EXPERIMENTAL

A frequency-response method was chosen for the measurement of axial mixing for two reasons. First, this technique offers advantages of simplicity over two other possible choices, namely, measurement of the response of the flow system to a concentration step function, in which the production of a sharp step exactly at the bed entrance is difficult, or measurement of axial mixing in the steady state, in which a tracer material must be introduced uniformly over the cross section of the flow system at the inlet and removed (e.g., by adsorption or chemical reaction) at the outlet. Second, a rapid gas-analysis system (*3*) was available which made possible measurements of concentration oscillations of as high as 20 cycles/sec.

Equipment

Figure 2 shows the flow system. Two gases pass through two stages of pressure regulation to rotameters. Needle valves downstream of the rotameters regulate gas flow to the concentration-wave generator. Leaving the wave generator, the mixed gas stream flows through a conical expansion section into the test column. Static pressure is adjusted with a valve beyond the column.

The gas pairs were hydrogen-nitrogen and ethylene-nitrogen. The electrical heater and room-temperature bath are used to bring the ethylene temperature, as measured by a thermometer in the gas line upstream of the flow meter, to within a few degrees of room temperature. Joule-Thomson cooling is not so severe with nitrogen and hydrogen so that the length of copper tubing between the pressure regulators and the flow meter offers enough heat transfer surface to assure these gases being at or near room temperature.

In addition to pressure reducers on the gas cylinder, diaphragm pressure regulators are installed upstream of the flow meters. Thus the flow-meter pressure could be kept constant for the entire range of flows required in the experiments. The flow meters are rotameters in banks of two (overlapping ranges) for each gas stream. They were calibrated against wet-test meters and a certified dry-gas meter. Calibrations were run with the meters at the same pressure as used in subsequent experiments. Corrections for small variations in room temperature and atmospheric pressure were made as directed by the flow-meter manufacturer.

The concentration-wave generator, shown in Figure 3, consists of a piston driven by a connecting rod from an eccentrically mounted pin on a flywheel. A connecting rod of sufficient length to ensure sinusoidal motion is used. The flywheel has adjustable counterweights mounted on its periphery to provide dynamic balancing. A sliding bar carrying the crank pin is bolted to the flywheel face, allowing changes in amplitude

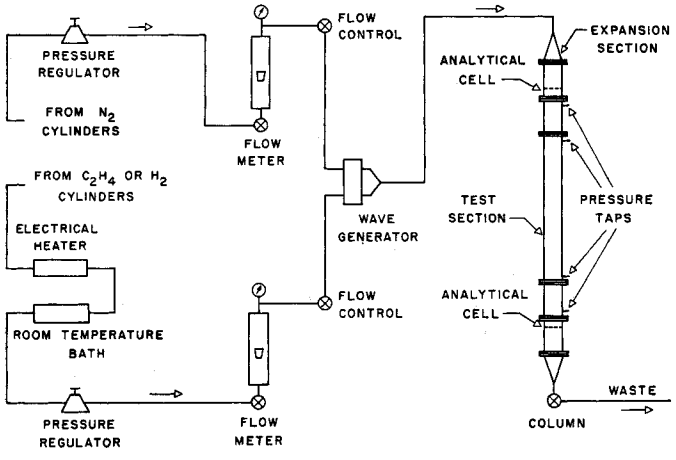

Fig. 2. Experimental flow system.

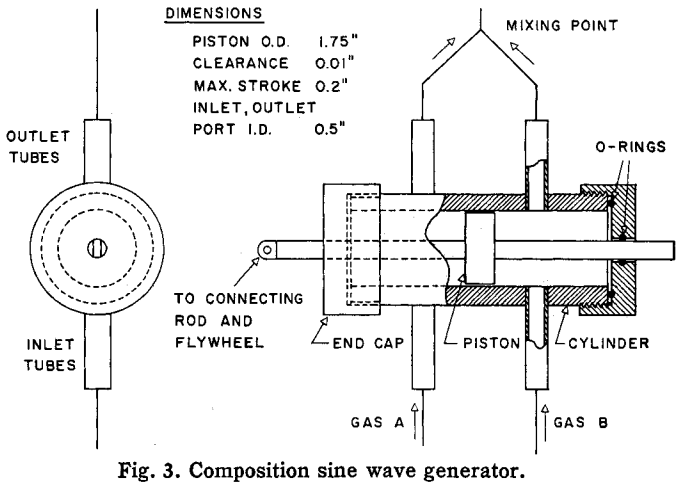

Fig. 3. Composition sine wave generator.

of the concentration wave. Through a variable-speed drive and interchangeable gears, a frequency range from a few cycles per minute to 30 cycles/sec. is available. Frequency is determined by timing a revolution counter geared to the flywheel shaft.

In operation, the motion of the piston, which does not travel far enough to reach the inlet and outlet ports, varies the capacity of the flow paths for the two gases in such a way that the concentration downstream of the mixing point is given by

$$x = x_M + \frac{\pi V f}{Q_T} \sin 2\pi f t \quad (27)$$

where x is the mole fraction of one gas in the binary mixture, x_M the mean mole fraction, V the volume displaced by a full stroke of the piston, f the frequency, Q_T the total volumetric flow rate, and t, time. Equation (27) was derived on the assumption of ideal gases. It was found that the amplitude of the concentration wave actually observed at the inlet of the test column was much less than $\pi Vf/Q_T$. This decrease was thought to be due to mixing in the flow system between the generator and the column, especially at the point where the flow area increased as the ⅛-in. connecting line met the column. A special conical expansion section was provided to decrease this mixing as much as possible. Although the loss in amplitude necessitated construction of a wave generator with four times the theoretical displacement volume, mixing which occurred in the approach lines assured damping of higher harmonics that might be present in the wave.

The column is comprised of seven sections flanged together. Following the expansion section is a 4-in. length of 2-in. Pyrex pipe. This section and a similar one at the lower end of the column carry the analytical cells and are packed above the top cell and below the bottom cell with the same packing material as the test section. Electrical leads for each cell are brought out between two layers of sheet rubber serving as gasket material for the upper and lower flanges. Coating the rubber with silicone fluid prevented current leakage to the grounded flanges due to moisture picked up from the surrounding air. Similar gasket material of single thickness is used for the remaining flanges.

The test section and the sections above and below it are made of 1.94-in. I.D. brass tubing. These three sections correspond to sections a, b, and b' in Figure 1. The length of b and b' is 0.5 ft., and test sections of 0.92, 1.99, and 2.91 ft. are available. Glass spheres 0.127 in. in diameter are used as packing for all sections. Micrometer measurements on sixty beads gave a standard deviation of 0.005 in. Fraction voids, as measured in the same column, are 0.388. The same method of packing, i.e., pouring a small volume of beads and tapping the column to promote settling, was used each time the column was repacked. A machined grid at the lower end of the bottom 6-in. section supports the packing, and a heavy screen held in place by a spring clip at the upper end of the top 6-in. section keeps the top level of the packing constant between repackings. No screens are used between the end sections and the test section and gaskets are cut to maintain a smooth wall across the joint. Pressure taps, located as shown in Figure 2, are connected to mercury manometers reading static pressure at the points indicated. Pressure drop across the test section could be correlated by use of Ergun's equation (5).

The rapid gas-analysis system used has been described in detail elsewhere (3). A radium-D source of alpha particles rolled onto a silver strip serves as one electrode of an ionization chamber. The strip is mounted axially in a brass cylinder, which is the other electrode and through which the gases to be analyzed flow. When a voltage is applied to the electrodes, an ion current flows which is directly proportional, over a short composition range, to the mole fraction of one of the gases in the mixture. A 100-megohm resistor between the center electrode and ground provides a voltage drop proportional to the current. Since the output impedance of the cell-resistor combination is very high, an impedance-matching circuit must be inserted between the resistor and a conventional cathode-ray oscilloscope. The circuit used in the triode-follower of Krakauer (6), with a balancing cathode-follower added to provide zero shift and minimize drift due to plate and filament battery-voltage changes. The necessary high-input, low-output impedance is provided by this circuit, which also has a frequency response flat to greater than 2,500 cycles/sec. In order to prevent stray capacitance from harming the frequency response, the cell leads were kept short by mounting a separate triode-follower for each cell at the point on the column where the lead emerged. A switching circuit allows the output from either triode-follower to be displayed on either a Leeds and Northrup Speedomax recorder or a DuMont 304A oscilloscope. The change in output for a 10 mole % change in gas composition is about 0.3 volt for both gas systems used. A fixed resistor voltage divider is used to attenuate the input to the recorder, which has a maximum range of 0 to 20 mvolt.

A disadvantage of the analysis system is the presence of a large amount of random noise in the ionization current. Three possible causes of this noise may be listed: trickle currents leaking between the high (−900 volts, outer electrode) and low-voltage (~ −3 volts, center electrode) portions of the cell; actual fluctuations in concentration within the cell; and random emission of alpha particles from the source. The possible presence of the first cause was shown by purposely adding moisture to the cylinder gases normally used, which led to a tenfold increase in noise. However, careful drying of the gases gave no improvement in noise level over that found when the gases were used directly from their cylinders. A simple guard ring made of a layer of grounded metal foil inserted between the two layers of Teflon separating the center electrode from the arm holding it, which is part of the outer electrode, was unsuccessful in lowering noise. Thus the first possible cause is either not important or cannot be eliminated by simple measures.

That turbulent concentration fluctuations do occur in a flowing system which has concentration gradients is certain; however, the noise level and noise frequency were the same in a quiescent as in a flowing system, and so the second possibility was eliminated.

The third cause, which was thought to be the major one, also could not be eliminated simply. Stronger radium-D sources than originally installed, 2.5 vs. 0.5 mcurie., improved the signal-to-noise ratio somewhat but still left the high noise level shown in Figure 4. The resulting increase in signal strength, however, made it possible to use a band-pass filter between the triode-follower and the oscilloscope. The filter used is a Krohnhite ultralow-frequency model with continuously variable upper and lower cutoffs. For the present use both upper and lower cutoff are set at the concentration-wave frequency. Since the cutoffs are not sharp, this practice results in some loss of signal but also in almost complete elimination of noise, even that at frequencies near the signal frequency. Figure 5 is the wave of Figure 4 after insertion of the filter. Noise *at* the signal frequency could not, of course, be repressed by this method. Because of this limitation, at the higher signal frequencies some variation in observed amplitude from wave to wave was noted, necessitating the averaging of amplitudes over several waves as described below. Noise amplitude below about two cycles per second is negligible, resulting in waves of uniform observed amplitude as shown by the one cycle per second waves in Figure 5. It should be noted that the use of the band-pass filter eliminates higher harmonics from the observed wave that may actually be present in the concentration wave. This is no way invalidates its use as long as the flow system is described by a linear differential equation. By superposition theory each concentration-wave frequency is attenuated as if it were present alone. That the flow system is linear is assured by the results, below, of experiments carried out at different concentration-wave amplitudes.

A further property of the analytical system is its pressure dependence. The ion current is directly dependent on the stopping power of the gas, which in turn depends on the pressure at constant temperature. Thus at constant composition more current is produced from the inlet cell than from the outlet cell owing to pressure drop across the intervening column. The same is true, to a lesser extent, with regard to the difference in current for a given concentration difference. Since it is this difference that is used as a measure of the concentration-wave amplitude, it is necessary to calibrate the cells under the same pressure conditions as those to be met in any given experiment with sinusoidally varying concentration. The technique of this calibration is discussed below.

Procedure

The data required for the determination of the axial Peclet number at any given Reynolds number can be conveniently divided into two static (without imposed concentration waves) and two dynamic (with imposed concentration waves) experimental results.

Static calibrations were run both with and without the test section of the column in place, as the pressure drop between the inlet and outlet cells was different in the two cases. Calibration factors in terms of change in cell output per unit change in gas composition for the inlet cell divided by the same ratio for the outlet cell were

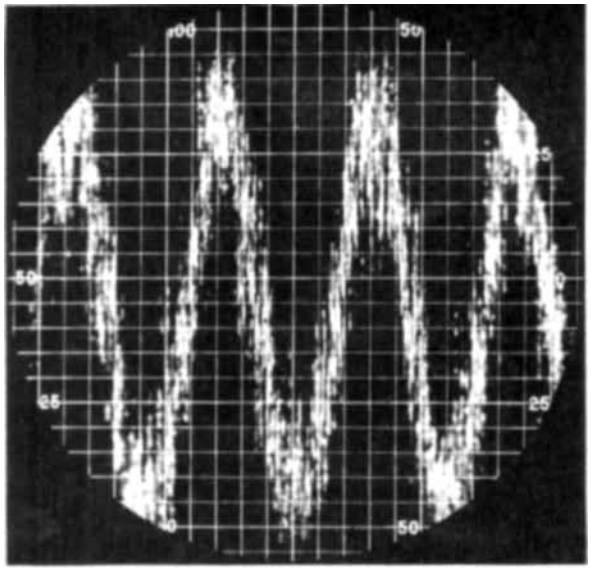

Fig. 4. Oscilloscope trace of one cycle per second concentration wave: unfiltered.

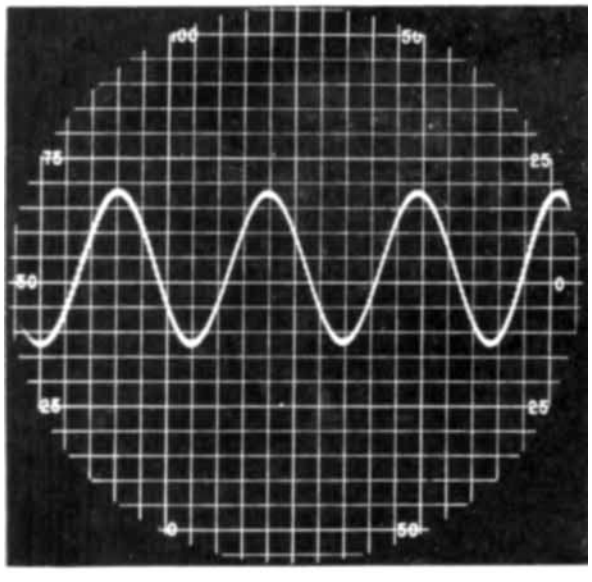

Fig. 5. Oscilloscope trace of one cycle per second concentration wave: filtered.

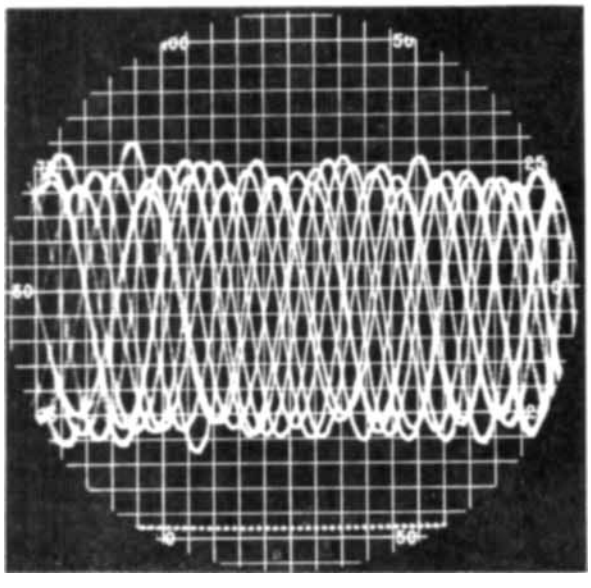

Fig. 6. Typical oscilloscope trace for concentration wave amplitude measurement.

obtained in the following manner. Flow rates of each of the two gases were set to the same value as that to be used in the succeeding dynamic experiment and the pressures of the two cells noted. With the cell pressures kept the same by increasing the flow of one gas while decreasing the flow of the other, the gas composition was changed by roughly 5 mole % from the mean composition to be used in the dynamic portion of the run. The output from each cell was set to near zero on the recorder. The gas composition was then adjusted, with the aid of the flow meters, to a value roughly 5 mole % on the other side of the mean. Since the change in gas composition was the same for both cells, dividing the output change for the inlet cell, as taken from the recorder chart, by the change for the outlet cell gave the desired factor. This procedure was repeated three times for each of the conditions (1) test section and end sections in place and (2) end sections only in place. The factors so obtained were always near unity and the 95% confidence limits for a typical mean of 3 were ± 0.04. Scatter was due to analytical cell noise and a certain amount of amplifier drift which could not be eliminated.

Dynamic runs were made under the same two conditions of test section in place and no test section as were the static runs. Preliminary tests were made to determine the proper length of wave-generator stroke to give about 10 mole % peak-to-peak waves at the inlet cell. The concentration amplitude of the inlet wave was determined by comparing the wave height on the oscilloscope face with a rough calibration of the oscilloscope similar to the static cell calibrations. No record of the inlet amplitudes for any given frequency and flow rate was kept, as initial experiments showed the Peclet number to be independent of amplitude. A single run usually covered a range of flow rates and always included three or more frequencies at each flow rate. Data were obtained for the various frequency-flow combinations in random order so as to include any unknown time-dependent effects with the experimental error. Replicates of each combination were made in all runs to give a good measure of this error.

Dynamic run procedure was as follows. After a suitable warm-up of electronic components the cell outputs were switched to the oscilloscope and the band-pass filter was adjusted to the desired frequency. The wave generator was started and frequency set by means of a Strobotac. An initial reading of the revolution counter was recorded and the stopwatch started. Gas flow was adjusted and readings of flow meters, cell pressures, test-section pressures, and room temperature recorded. With the inlet-cell output shown on the face of the oscilloscope a photograph of the trace was taken. This was repeated for the outlet cell, flows were rechecked, and the final reading of the revolution counter and elapsed time were recorded.

Figure 6 shows a typical photograph of the oscilloscope trace. By operating the oscilloscope so that the signal was slightly out of synchronization with the sweep, multiple exposures could be made in which individual waves did not superimpose and could be picked out for amplitude measurement. In the section of Figure 6 covered by the center fifty horizontal units, twenty waves can be distinguished. Averaging the maxima and minima of these waves gives an average amplitude of 52 ± 1 at a 95% confidence level. The variation in amplitude from wave to wave is caused by random noise at the same frequency as the signal frequency.

As the phase angle does not contain the

diffusivity until higher order terms than those in Equation (6) are reached, phase-angle measurements do not provide an accurate method of determining axial Peclet numbers. However, in a few runs phase angles were measured as a check on the validity of Equation (6). Lissajous patterns on the oscilloscope were used in phase-angle determination. At a given flow rate frequencies were adjusted to give the easily discernible patterns of 90, 180, 270, and 360 deg. Frequency, flow rates, and pressures were recorded to allow calculation of phase angles for comparison with the measured angles.

Treatment of data consisted of the following three operations: calculation of Reynolds number, calculation of Peclet number, and, where applicable, calculation of phase angle.

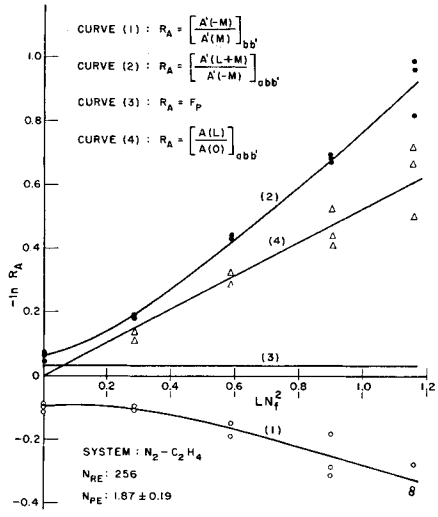

Fig. 7. Example of relative importance of various experimental corrections.

Reynolds number was calculated from the measured flow rates converted to mass velocity in the unpacked column, measured particle diameter, and viscosity as determined by the Wilke (*11*) correlation for gas mixtures. All values were taken at the mean gas composition.

Peclet number was calculated as follows. By comparison of the photographs of the traces from inlet and outlet cells amplitude ratios $[A(L + M)/A(-M)]_{abb'}$, from the portion of the run with test section in place, and $[A(-M)/A(M)]_{bb'}$, from the portion with only end sections in place, were determined for each frequency-flow combination. Since replicates of each combination were made, a pair of each of the ratios was calculated. Based on the original random order of data taking, a random choice of the two ratios to be used together as in Equation (18) was made. With this method of calculation a fair picture of the experimental error in both portions of the dynamic runs is reflected in the final Peclet numbers. Consistent use of the high values of one ratio with the low values of the other would have unduly minimized error, and pairing high with high and low with low would have increased the spread of Peclet numbers beyond the true error. To convert the amplitude ratios as measured in oscilloscope units to the corresponding concentration ratios, use was made of the results of the static calibrations. The factor $[\Delta R_{in}/\Delta R_{out}]_{abb'}$, which is the change in recorder output for unit change in mole fraction for the inlet cell divided by the same ratio for the outlet cell, when multiplied by the measured amplitude ratio with the test column in place gives that amplitude ratio in concentration units. The similar factor from the static calibration with end sections only multiplied by the corresponding amplitude ratio gives that ratio in concentration units. In practice the logarithms of the two amplitude ratios were determined along with that of the pressure correction and the three added to give the desired amplitude ratio:

$$\ln\left[\frac{A(L+M)}{A(-M)}\right]_{abb'} + \ln\left[\frac{A(-M)}{A(M)}\right]_{bb'} + \ln F_p = \ln\left[\frac{A(L)}{A(0)}\right]_{abb'} \quad (28)$$

where

$$F_p = \frac{[\Delta R_{in}/\Delta R_{out}]_{abb'}}{[\Delta R_{in}/\Delta R_{out}]_{bb'}} \quad (29)$$

The use of recorder units in the case of the static factor and oscilloscope units in dynamic amplitude ratios is not inconsistent, as both measure voltage. The factor relating the two measurements is constant and cancels when used in ratios. The negative of the right-hand side of Equation (28) is the experimental ordinate of the plot described by Equation (8). The abscissa, N_f^2L, was calculated directly from experimental values of flow rate, converted to velocity by use of the density of the mean gas mixture at the mean column pressure, frequency, particle diameter, and test-section length.

The plot of Equation (8) having been formed for each value of Reynolds number, the slope, $1/N_{Pe}'$, and the 95% confidence limits on the slope were determined from a least squares fit of the data. Taking the reciprocal of the slope gives the Peclet number and expressing the confidence limits as percentage of slope equals percentage of Peclet number gives the limits on the Peclet number.

Runs involving phase-angle measurement were made before the indirect method of amplitude-ratio measurement was developed. This is not a drawback to the validity of the results, however, for two reasons. First, as has been mentioned, under the conditions in which the expansion of Equation (4) to Equation (5) is allowable, phase angle is not a function of axial mixing; hence the unknown amount of mixing caused by entrance and exit effects is not a factor. Second, a correction involving the transit time of a wave through the analytical cells can be applied to take into account the finite thickness of the cells. The objections to the use of the direct method which were raised in the case of amplitude determination are thus circumvented. Phase-angle calculations then simply involve comparison of measured phase angles with the calculated values, N_fL, corrected for cell transit time. The correction is

$$\phi_{trans} = \frac{\omega L_c}{2}\left[\frac{U_{in} + U_{out}}{U_{in}U_{out}}\right] \quad (30)$$

where ϕ_{trans} is the phase angle due to transit time of one-half inlet cell + one-half outlet cell, L_c is the length of each cell, and U the velocity through the cell calculated from the flow rate and density at the cell pressure. Then

$$\phi_{calc} = N_fL + \phi_{trans} \quad (31)$$

RESULTS

The variables investigated in determining the correlation of Peclet number vs. Reynolds number and the ranges covered are shown in Table 1.

TABLE 1

VARIABLES INVESTIGATED

Variables of measuring technique	Range
1. Frequency	0.21–10.4 cycles/sec.
2. Amplitude	5 and 10 peak-peak mole %
3. Column length	0.92, 1.99, 2.91 ft.
Variables affecting axial diffusion	
1. Reynolds number	10.4–379
2. Gas system	C_2H_4—N_2, H_2—N_2
3. Mean composition of gas	20, 50 mole % C_2H_4 50 mole % H_2

Factors affecting axial mixing which were held constant were column diameter, 0.161 ft.; packing type, spherical random; and packing diameter, 0.0106 ft.

Confirming Experiments

Several experiments were performed to check the validity of the use of an equation based on Fick's Law, Equation (1), to describe axial mixing in packed beds, and to determine whether the indirect method of amplitude ratio measurement summarized in Equation (18) was effective in eliminating end effects. The criteria for validity of Fick's Law were (1) linearity and zero intercept of the plot of $-\ln [A(L)/A(0)]_{abb'}$ vs. LN_f^2, (2) independence of calculated Peclet numbers from initial concentration wave amplitude, Equation (1) being a linear differential equation, and (3) agreement between calculated and measured phase angles. Criteria for the soundness of the experimental method also included amplitude independence as well as independence of the Peclet number of the column length.

A typical plot of $-\ln [A(L)/A(0)]_{abb'}$ vs. LN_f^2 is shown in curve 4 of Figure 7. The actual variable in the abscissa is the frequency, as column length, particle diameter, and flow rate were kept constant throughout the experiment. The plotted points determining curve 4 result from the random combinations of

points at the same abscissa from curves 1 and 2, as mentioned above, plus the constant pressure and cell strength correction shown in curve 3. The results of the static calibrations for the flow conditions shown are plotted on the ordinate. Since the correction factor, F_p, is determined from the same static calibrations, addition of curves 1, 2, and 3 *at the origin* gives curve 4 a zero intercept by definition. For this reason no points are plotted for curve 4 on the ordinate and only the triangular points shown were used in checking the validity of Fick's Law.

A general equation for the best line through the ten points may be written:

$$-\ln\left[\frac{A(L)}{A(0)}\right]_{abb'} = a + b_1(LN_f^2) + b_2(LN_f^2)^2 + b_3(LN_f^2)^3 + \cdots \quad (32)$$

where a, b_1, b_2, . . . are coefficients to be determined by least squares. Forming the least squares quadratic one obtains

$$-\ln\left[\frac{A(L)}{A(0)}\right]_{abb'} = -0.0313 + 0.543(LN_f^2) + 0.0275(LN_f^2)^2 \quad (33)$$

The linear regression line may also be determined:

$$-\ln\left[\frac{A(L)}{A(0)}\right]_{abb'} = -0.0432 + 0.583(LN_f^2) \quad (34)$$

And, finally, the best straight line through the origin is determined:

$$-\ln\left[\frac{A(L)}{A(0)}\right]_{abb'} = 0.536(LN_f^2) \quad (35)$$

An analysis of variance which tests the difference between deviations from the lines represented by Equations (33) and (34) against the deviations from the quadratic indicates that the quadratic term is not significant at the 75% level. A similar test of the difference between deviations from Equations (34) and (35) against deviations from Equation (34) shows no significance of the nonzero intercept at the 75% level. The 75% confidence level was chosen rather than the more usual 95% level to ensure that if a quadratic term or a nonzero intercept were present in the data they would not be missed by requiring 95% certainty of their existence. Similar checks made on all experiments substantiated the assumption that within the precision of the data the plots of amplitude ratio vs. LN_f^2 were linear with zero intercept.

A complete factorial design of experiments covering several initial amplitudes, the three available column lengths, and the entire Reynolds number range was not a feasible method of determining whether the assumptions of amplitude independence and column-length independence were valid. Instead, one experiment was designed to check the amplitude effect and another the column-length effect, both being run at the same Reynolds number. In addition, simultaneous checks were made on the effect of interchanging the two analytical cells, which are identical in dimensions and differ only in the strength of the radium-D alpha-particle sources, one being about 6% stronger than the other.

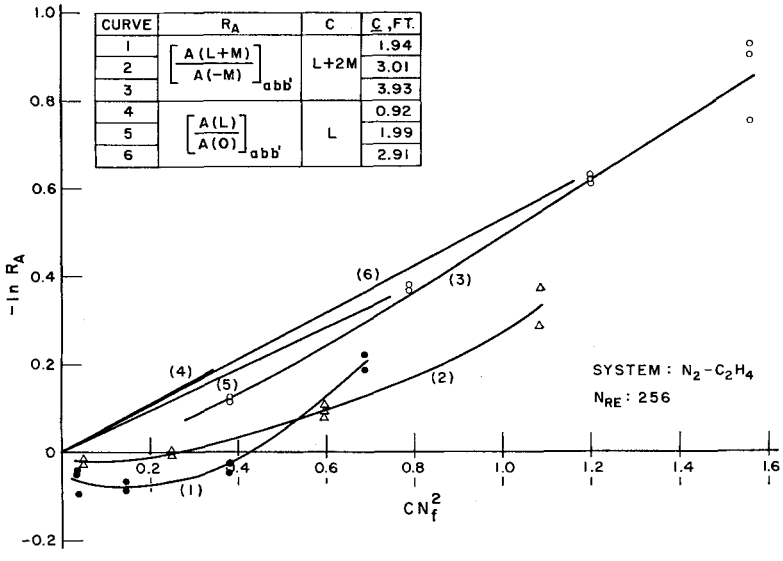

Fig. 8. Experimental demonstrations of effectiveness of correction for end effects.

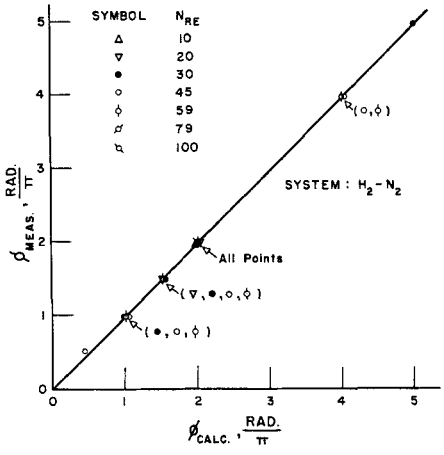

Fig. 9. Comparison of measured and calculated compositional phase angles.

Table 2 shows the results of the experiments designed to confirm the assumptions of the theory and the experimental method.

The details of statistical computations are reported elsewhere (*9*). The conclusion reached from the statistical calculations is that there are no significant effects of column length, initial amplitude, and analytical cell strength on the Peclet numbers determined in the runs shown in Table 2. All remaining runs were made with the longest column, approximately 10 mole % peak-to-peak initial amplitude, and analytical cells in the "normal" positions.

Figure 8 is another demonstration of the effectiveness of the correction for end effects embodied in the indirect method of amplitude measurement. Curves 1, 2, and 3 show the observed amplitude ratios plotted against N_f^2 times total column length (test section plus end sections) for the three columns used. These plots represent the data uncorrected for end effects. However, curves 4, 5, and 6 show the least square lines through the same data to which the corrections derived from measurements

TABLE 2

RESULTS OF CONFIRMING EXPERIMENTS*

Run	Amplitude†	Test-section length, ft.	Cell positions‡	Peclet number	Limits** on N_{Pe}'
E-34	High	2.91	Normal	1.32	±0.12
E-35A	High	0.92	Normal	1.83	±1.49
E-35B	High	1.99	Normal	2.14	±0.42
E-37H	High	2.91	Reversed	2.14	±0.27
E-37L	Low	2.91	Reversed	2.30	±0.53
E-38	High	2.91	Reversed	2.28	±0.26
E-40	High	2.91	Normal	1.87	±0.19
			Mean	1.98	±0.32††

*N_{Re} = 256, 20 mole % C_2H_4 in N_2 for all runs.
†High amplitude = approximately 10 mole % peak to peak. Low amplitude = one-half high amplitude.
‡Normal = cell with stronger source at column inlet.
**95% confidence.
††Limits on a mean of seven runs.

with end sections alone are applied. The Peclet numbers listed in Table 2 for runs E-35A, E-35B, and E-40 were calculated from the slopes of curves 4, 5, and 6, respectively. It may be seen that the end-effect correction is greatest for the shortest column (cf. curves 1 and 4) and least for the longest column (cf. curves 3 and 6). This type of behavior is expected.

The effect of pressure drop and the resulting difference in mean gas density between inlet and outlet of the test section was not tested experimentally. However, an approximate solution of Equation (1) with sinusoidal boundary conditions in which the velocity U was replaced by G/ρ and ρ was allowed to vary with distance was formulated. No significant effect of pressure drop on amplitude ratio, for a given Peclet number, in the range of pressure drops met with in the present work was found. (Maximum density difference between inlet and outlet of the test section was 14.5% for the H_2—N_2 system and 12.2% for the C_2H_4—N_2 system.) Hence, it is believed that pressure drop has no effect on the validity of the experimental method.

The final point in the proof of the validity of Fick's Law for packed beds is the correlation of measured and calculated phase angles in Figure 9. While the excellent agreement does not exclude the possibility that a packed bed follows a non-Fickian law, if it does follow Fick's Law the correlation is required.

The conclusions reached from the confirming experiments are these:

1. The experimental method provides reliable estimates of a parameter, the Peclet number, in the Fick's-Law equation for axial diffusion in a packed bed.

2. This equation, while giving no insight into the details of axial mixing, is a sufficiently precise means for describing the gross behavior of such a bed.

Prime Results

The final correlation of Peclet number and Reynolds number is shown in Figure 10. The ordinate is Peclet number, written $d_p\ U/D + E$, where d_p is particle diameter, U is interstitial velocity, E is eddy diffusivity, either axial or radial, and D is molecular diffusivity. The ordinate is Reynolds number d_pG_0/μ, where G_0 is superficial mass velocity, based on the empty-column cross section, and μ is viscosity. The choice of a log-log plot is based on ease of data presentation only.

Precision of the present data is indicated by a vertical line joining two plotted points which represent the 95% confidence limits on the Peclet number value for each experiment. The precision indicated is believed to be due primarily to random noise in the analytical system.

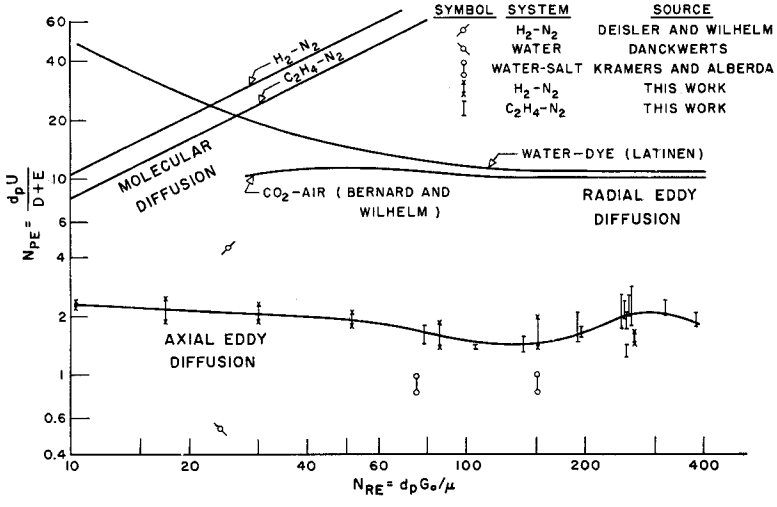

Fig. 10. Diffusion in packed beds in terms of Peclet number vs. Reynolds number.

Each pair of points represents a determination of Peclet number based on a slope such as in Figure 7, and includes at least twelve amplitude-ratio measurements, six on test column plus end sections and six, for calibration purposes, on end sections alone. At least three different frequencies, with replication of each, were involved.

The effect of Reynolds number may be seen in the line drawn through the plotted points. The curvature shown is perhaps arbitrary. However, under the assumption that axial and radial mixing are similar processes a break in the curve in the 100 to 200 Reynolds-number range might be expected. An alternative procedure is to find the best straight line through the plotted points by least squares. This line is found to have essentially zero slope, and hence a mean of all values may be used. An exact statement as to the significance of this mean follows.

For twenty-one determinations of Peclet number in the Reynolds-number range from 10 to 400: $Pr\ (2.03 > \nu_{Pe} > 1.73) = 95\%$, where Pr is read as "the probability of" and ν_{Pe} is the true mean of twenty-one determinations.

The effect of gas system may be noted by comparing the points shown for the two systems tested. In the Reynolds-number range where the data overlap, no significant difference exists between Peclet numbers for the 20 mole % C_2H_4 in N_2 and 50 mole % H_2 in N_2 systems. In addition, the Peclet number for the 50 mole % C_2H_4 in N_2 system was determined at $N_{Re} = 191$. It was found to be the same, within experimental error, as that for the 20% C_2H_4 mixture at $N_{Re} = 194$. The 50% C_2H_4 data were less precise because of a higher noise level in the analytical-cell output at the higher C_2H_4 concentration. It may be inferred that there is no major effect of gas composition on Peclet number. In comparing the two gas systems tested it is well to note that there is a fourteenfold density difference between nitrogen and hydrogen, whereas the densities of nitrogen and ethylene are the same. Thus any effects of density difference on axial mixing may be ruled out, at least in the overlapping Reynolds-number range. Extension of the correlation to untested gas pairs therefore may be made with more assurance.

DISCUSSION

A graphical comparison of data of three other investigators with present measurements of axial Peclet numbers is given in Figure 10. The experimental method of Deisler and Wilhelm (4) most closely approximates that of this work. The same analytical system as well as frequency-response technique was used. The axial Peclet number shown here was calculated from their value of D_L, the longitudinal diffusivity, measured over the Reynolds-number range from 3.8 to 48.4, and is plotted vs. the mean N_{Re}. In their work prime interest was in measuring the intraparticle diffusivity of porous pellets. The value of longitudinal diffusivity was a by-product of the main work and could be obtained only as a single value characteristic of a range of Reynolds numbers. It is believed that the present method, in which there is no added effect of porous packing, has more utility for axial-diffusion measurements as such.

Kramers and Alberda (7) also used the frequency-response method. In their system the sinusoidally varying salt concentration was followed by means of electrical conductivity. The packing consisted of Raschig rings and there was a particle-to-tube ratio of 0.13 and a length-to-diameter ratio of 4.6. The equation solved by these authors and its approximate solution were the same as Equations (1) and (6), respectively, although different boundary conditions were used. The Peclet numbers shown in Figure 10 were calculated from their values of D/Ud_p, where D is axial diffu-

sivity. The limits of accuracy and the Reynolds number range over which these authors state that the Peclet numbers are valid are shown in the figure. It would be fortuitous if these data, for a liquid system, agreed exactly with those for gas systems. However, it may be pointed out that it was found in the present work that short columns gave incorrect results owing to end effects. In addition, the high particle-to-tube ratio and the hollow packing might lead to extensive by-passing. The effect of by-passing would be to show more axial mixing and hence a lower N_{Pe} than was found in the present investigation.

The value of Peclet number for a Reynolds number of 24 calculated from the data of Danckwerts (*2*) also is shown. In Danckwerts's work an equation similar to Equation (1) was solved for a concentration step introduced at zero time at the inlet of the bed. Axial diffusivity could then be calculated by matching experimental outlet concentration vs. time curves with those given by the solution to the equation. The lack of agreement between these and present data may be due to differences in system alone. Here too, however, Raschig rings were used in a column of such size that the particle-to-tube ratio was 0.20. By-passing might account for the low value observed.

It is interesting also to compare axial mixing with the data in the literature on radial mixing. A radial Peclet number of about 12 in the Reynolds-number range from 100 up has been found by several investigators, and curves for two cases (*1*, *8*) are shown in the figure. Present data indicate that axial mixing is about six times as efficient as radial mixing in a packed bed. It is presumed that axial mixing is the consequence of more complex events, such as local trapping, by-passing, acceleration, and deceleration, than the stream-splitting, or "random-walk," mechanism that has served well in explaining radial mixing. Implications of more efficient axial mixing to the designer of chemical reactors are, however, apparent. In most reactor designs axial diffusion is neglected because axial gradients are not steep. This may, in some cases, be an unsafe assumption, as even a small gradient multiplied by a large coefficient in a differential equation can lead to an important element in the solution of the equation.

The curves for molecular diffusion for the two gas systems make up the final portion of Figure 10. These curves serve to point out the greater than thirtyfold increase in axial mixing efficiency for a turbulent system in the N_{Re} range from 100 up. If other effects, such as natural convection, could be eliminated at very low flows, it would be expected that the curves for eddy and molecular diffusion would merge at a low value of Reynolds number.

A final comparison is made between the Peclet numbers obtained in this work and the number predicted when it is assumed that as each particle of packing is traversed complete mixing takes place. The excellent agreement found between the predicted value of 2.0 and the experimental of 1.88 $\pm$ 0.15 is suggested to provide a basis for still further and more detailed investigations of fundamental aspects of mixing.

An assessment of the importance of axial mixing in chemical reactors has not yet been completed.

ACKNOWLEDGMENT

The authors express their appreciation to the General Electric Company, the duPont Company, and the Shell Development Company for support of graduate fellowships during the course of this work.

The authors wish also to acknowledge with thanks guidance provided by Professor J. C. Whitwell in statistical aspects of the work.

NOTATION

Dimensions of the quantities listed are given as m = mass, l = length, t = time. Any consistent system may be used.

$a, b_1, b_2, \ldots$ = coefficients in regression equations
c_1 = inlet concentration to perfect mixer, moles/l³
c_o = uniform concentration within perfect mixer, moles/l³
d_p = packing element diameter, l
f = frequency, t⁻¹
f = function of
f_{in} = function of for inlet analytical cell
f_{out} = function of for outlet analytical cell
n = number of perfect mixers in series
t = time, t
x = mole fraction
x_M = mean mole fraction about which concentration oscillates
$\mathbf{x}$ = complex mole fraction
$\mathbf{z}$ = axial coordinate, l
A = amplitude of concentration wave, mole-fraction units
A_n = amplitude of concentration wave in nth perfect mixer of series, moles/l³
A_0 = amplitude of concentration wave entering first perfect mixer of series, moles/l³
$\mathbf{A}$ = complex amplitude
D = molecular diffusivity, l²/t
E = eddy diffusivity, l²/t
E_z = eddy diffusivity, axial direction, l²/t
F_p = pressure and cell strength correction for analytical system, dimensionless
G = mass velocity, based on interstitial area, m/l²t
G_0 = mass velocity, based on empty-column cross section, m/l²t
L = dimensionless bed length = $\mathbf{L}/d_p$
$\mathbf{L}$ = bed length, l
L_c = length of analytical cell, l
M = dimensionless length of end sections = $\mathbf{M}/d_p$
$\mathbf{M}$ = length of end sections, l
N_f = frequency number = $d_p\omega/U$
N_{Pe}' = Peclet number, axial direction = d_pU/E_z
N_{Pe} = generalized Peclet number = $d_pU/(E + D)$
N_{Re} = Reynolds number = d_pG_0/μ
Q_T = total volumetric flow through wave generator, l³/t
R_A = amplitude ratio, dimensionless
ΔR_{in} = change in output of inlet analytical cell for unit mole percentage of change in gas composition, volts/mole %
ΔR_{out} = ditto for outlet cell
U = interstitial velocity, l/t
V = volume displaced by full stroke of wave generator piston, l³
λ = length assigned to single perfect mixer, l
μ = viscosity, m/lt
ν_{Pe} = true mean axial Peclet number
ρ = density, m/l³
ϕ_{calc} = calculated phase angle, radians
ϕ_{meas} = measured phase angle, radians
ϕ_{trans} = phase angle due to transit time of concentration wave through analytical cells, radians
ψ_{in} = variable characterizing mixing in inlet analytical cell
ψ_{out} = ditto for outlet cell
ω = angular frequency, radians/t

Subscripts

a, b, b' = sections of column (Figure 1) in place when measurements are made

LITERATURE CITED

1. Bernard, R. A., and R. H. Wilhelm, *Chem. Eng. Progr.*, **46**, 233 (1950).
2. Danckwerts, P. V., *Chem. Eng. Sci.*, **2**, 1 (1953).
3. Deisler, P. F., Jr., K. W. McHenry, Jr., and R. H. Wilhelm, *Anal. Chem.*, **27**, 1366 (1955).
4. Deisler, P. F., Jr., and R. H. Wilhelm, *Ind. Eng. Chem.*, **45**, 1219 (1953).
5. Ergun, Sabri, *Chem. Eng. Progr.*, **48**, 89 (1952).
6. Krakauer, Stewart, *Rev. Sci. Inst.* **24**, 496 (1953).
7. Kramers, H., and G. Alberda, *Chem. Eng. Sci.*, **2**, 173 (1953).
8. Latinen, G. A., Ph.D. dissertation, Princeton Univ., Princeton, N. J. (1951).
9. McHenry, K. W., Jr., Ph.D. dissertation, Princeton Univ., Princeton, N. J. (1957).
10. Ogburn, Hugh, Ph.D. dissertation, Princeton Univ., Princeton, N. J. (1954).
11. Wilke, C. R., *J. Chem. Phys.*, **18**, 517 (1950).
12. Rosen, J. B., and W. E. Winsche, *J. Chem. Phys.*, **18**, 1587 (1950).

Presented at A.I.Ch.E. Pittsburgh meeting